Article

The Potential of Fully Polarized ALOS-2 Data for Estimating Forest Above-Ground Biomass

Zhihui Liu [1], Opelele Omeno Michel [1,2], Guoming Wu [1], Yu Mao [1], Yifan Hu [1] and Wenyi Fan [1,*]

1   Key Laboratory of Sustainable Forest Ecosystem Management—Ministry of Education, School of Forestry, Northeast Forestry University, Harbin 150040, China; liuzh@nefu.edu.cn (Z.L.); michel.opelele@unikin.ac.cd (O.O.M.); wgm@nefu.edu.cn (G.W.); maoyu@nefu.edu.cn (Y.M.); yifan_hu2021@nefu.edu.cn (Y.H.)
2   Department of Natural Resources Management, Faculty of Agricultural Sciences, University of Kinshasa, 117 Kinshasa XI, Mont-Amba District, Kinshasa 01031, Congo
*   Correspondence: fanwy@nefu.edu.cn; Tel.: +86-139-4605-0384

Abstract: SAR data have a longer wavelength and stronger penetrating power compared with traditional optical remote sensing. Therefore, SAR data are more suitable for the estimation of the above-ground biomass (AGB) of forests. This study was aimed at evaluating the sensitivity of L-band full polarization data to AGB. L-band data were improved to estimate the saturation point produced by AGB, and were found to be suitable for estimating a wide range of AGB. This study extracted backscattering coefficients, polarization decomposition variables, and terrain factors. New parameters were constructed from these variables, and their performance in predicting AGB was evaluated. Significant variables found with AGB were added to the multivariate linear model. A statistical analysis showed the presence of multicollinearity between the variables. Therefore, ridge regression, random forest method (RF), and principal component analysis (PCA) were introduced to solve the problem of collinearity. In all the three methods, the saturation of the ridge regression model was low, reaching it at 150 t/ha. Better accuracy was obtained with the RF model. No obvious saturation incident was detected in the model established using the principal component analysis. This could be attributed to the low biomass levels observed in our study area. This model provided accurate results (adjusted r^2 = 0.90 rmse = 14.24 t/ha), indicating that L-band data have the potential to estimate AGB. Additionally, suitable variables and models were selected in this study, with the principal component analysis being more helpful in combining various SAR parameters. The achievement of these accurate results could be attributed to the synergy among variables.

Keywords: backscatter coefficients; polarization decomposition; collinearity; ridge regression; RF; PCA

1. Introduction

Carbon sequestration capacity is an important manifestation of forest functions. Forest above-ground biomass (AGB) is a consequential evaluation index of carbon sequestration capacity. Therefore, it is necessary to estimate AGB to understand the carbon sequestration capacity in a particular area [1]. Previous studies have shown that the use of the backscatter coefficient of airborne L-band SAR data could not significantly improve the ability to estimate AGB [2]. In large survey areas, the AGB root mean square error (RMSE) estimated from HH polarization has been found to be about 30% [3,4]. Similarly, the use of L-band data to predict the Indian tropical forest had a higher accuracy with RMSE = 16.06 t/ha [5]. Previous studies have used the random forest (RF) method to estimate the AGB with RMSE = 18.9 t/ha. Additionally, a regression model was built to estimate the boreal forest AGB with RMSE = 37.3 t/ha [6,7]. These studies obtained tree height by laminar analysis of SAR data and then calculated AGB with RMSE = 36.3 t/ha [8]. However, different AGB estimation methods have been found to provide discordant results even when the same SAR data are analyzed. Meanwhile, variability of forests has been found to be among the factors

affecting the accuracy of AGB estimation. Several studies have estimated the forest biomass of tree trunks using radar backscatter coefficients. The sensitivity of the radar backscatter coefficients to AGB depends on the wavelength; the longer the wavelength, the higher the sensitivity [9,10]. A National Aeronautics and Space Administration (NASA) study in Landers Pine Forest showed that the dynamic range of the radar backscatter coefficient was greater in the P-band, followed by the L-band, which had the highest HV polarization and VH polarization sensitivity [11,12]. HH polarization has been found to be suitable for sparse areas, while HV polarization is suitable for dense areas [13]. The use of radar data to estimate the AGB of planted forests tends to have more accurate estimations than in other forest types [14,15]. However, the applicability of this method in natural forests is still uncertain. Previous studies have estimated a saturation point when using backscatter coefficients to estimate forest biomass, and reasonable results have been achieved when the biomass is less than 150 t/ha [16]. Lower saturation points have been recorded in AGB of complex tropical forests and different forest types, while pure forests and swampy areas have shown higher saturation points [17,18]. This suggests that the difference in estimated AGB saturation point is affected by area, forest density, and tree species composition. The ratio combination of different polarization channels increased the saturation point when estimating AGB, leading to more accurate results [19,20]. Meanwhile, the ability to estimate AGB using radar backscatter coefficients has been found to be limited [21]. In addition, this method of estimating AGB has a lower saturation point, which limits its application.

Other reasons that affect the accuracy of AGB estimates include model variability and different parameters. Some previous studies have not discussed the synergistic effects when estimating AGB using backscattering coefficients or decomposition parameters. Improving the saturation point of the estimated AGB has also been difficult. However, some polarization decomposition methods have proved suitable for estimating the AGB of forests. Three simple scattering mechanisms have been used to describe SAR observation results. These mechanisms achieved acceptable accuracy, which proved that the decomposition method is suitable for estimating vegetation biomass [22,23]. The azimuth offset compensation of SAR data before polarization decomposition partially improves the accuracy of AGB estimation [24]. In addition, the VanZyl three-component decomposition and Yamaguchi three-component decomposition obtain more accurate results [25,26]. The polarization decomposition method estimated a higher saturation point for AGB than the backscatter coefficient. Most researchers have used linear and nonlinear regression models to predict AGB [27–31]. Although these studies have optimized the model, there has been limited focus on the parameters. Meanwhile, the accuracy obtained by using different decomposition methods to estimate AGB varies greatly [32–34]. This shows that different polarization decomposition methods are suitable for different types of ground features. However, combining the polarization decomposition parameters and the water cloud model to predict AGB achieves better results [35]. Additionally, the use of multiple polarization decomposition parameters to establish a multivariate model could slightly improve accuracy [36]. The RF method has been found to obtain accurate results in estimating AGB [37–39]. However, its applicability to small sample sizes remains uncertain. Therefore, the choice of the model is an important factor affecting accuracy.

Previous studies did not select the most suitable variables for forest AGB estimation. In addition, there is still lack of in-depth studies on the relationships between variables, making it difficult to reasonably utilize SAR data. As such, it is difficult to improve the saturation point of the estimated AGB.

At present, AGB can be estimated using long-band SAR data, although the saturation points and estimation accuracy can still be improved. The present study not only estimated the AGB based on backscatter coefficient and polarization decomposition parameters, but also combined the two to establish the potential of long-wavelength full-polarization data to estimate forest biomass. Unlike previous studies, this study used variables from SAR data to construct parameters that were more sensitive to AGB. All variables that were

significantly related to AGB were combined. A model that was more suitable for the estimation of AGB was also selected.

Specifically, this study was aimed at:

(1) Using the original channel backscatter coefficients to establish a univariate model to estimate AGB. The ratio of backscatter coefficients was calculated and a univariate model established. The impact of topographical factors on AGB was also analyzed.

(2) Selecting the most suitable polarization decomposition method and polarization decomposition parameters. Polarization decomposition parameters were used to construct a stronger estimation ability for the new parameters, and a model was established with AGB.

(3) Comparing the ability of ridge regression, RF and the PCA method to resolve a high-dimensional variable set. The focus was on establishing a model, and predicting the AGB at the regional scale by using all the relevant parameters.

2. Study Area and Data

2.1. SAR Data

The SAR data used in this study were the ALOS-2 PALSAR full-polarization observation data obtained on 8 August 2020. The selected image covered northern China (Figure 1). The image is from a 1.1-level L-band radar developed by the Japan Aerospace Exploration Agency (JAXA). The average zenith angle was 27.8°, the radar center frequency was 1.27×10^3 MHz, the range resolution was 5.66 m, and the azimuth resolution was 2.86 m. The pixel size was 16.19 m^2. The overall observation area was 4494.62 km^2, and the average height of the sensor from the Earth's surface was 634.24 km^2.
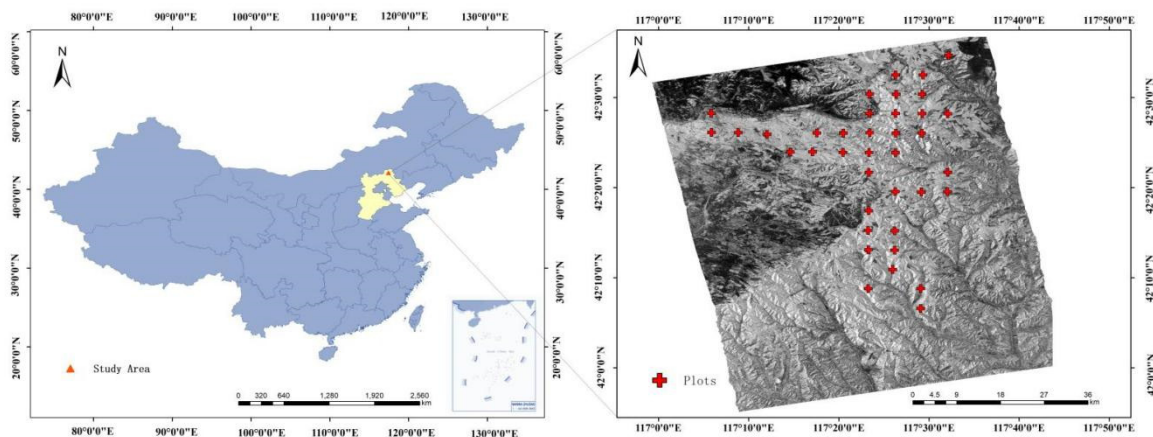
Figure 1. SAR data illustration of sample sites.

2.2. Field Data

The study area was a typical temperate forest in northern China. The forest is located in Hebei Province, North China (117E, 42N). This area is located in the transition zone from Yanshan Mountain to Inner Mongolia. Except for the mountain, the rest of the area consists of plains and cities. Altitude ranges from 1171 m to 1960 m asl. This area is characterized by a mixed forest of coniferous and broad-leaved trees, with North China larch (*Larix principis-rupperchtii* Mayr) and white birch (*Betula platyphylla* Suk) being the main species. A total of 38 fixed plots were used in the image. The field data used in this study were obtained through field surveys in 2020. In order to avoid interference, the measurements were carried out at a distance of more than 30 m from non-forest areas. Field surveys included measuring tree species composition, and measuring diameter at breast height (DBH) at a distance of 1.3 m from the ground. All trees with a DBH of less than 2.5 cm were eliminated. Tree height was measured using Vertex IV and Transponder T3. The coordinates of the center point of the plot were determined using the Unistreng RTK-G10.

We ensured that the center point coordinate error of the sample plot was within 10 cm. The individual allometry equation of local tree species was used to calculate the AGB of the forest for each sample [40,41]. Based on the measured results, the minimum biomass above the forest was 4.24 t/ha and the maximum was 185.08 t/ha. The plots were separated at equal intervals, and each plot had an area of 0.06 ha. The shape of each set of field data was a rhombus, with a diagonal length of 17.3 m. The area of the plot was 149.645 m^2. The AGB level in this area was found to be more suitable for this study. Meanwhile, microwave remote sensing observation methods were more suitable for forest biomass estimation, considering the complex geological and climatic conditions in the area. The actual biomass is shown in Table 1.

Table 1. Statistical data of the plots.

Number	AGB (t/ha)	Number	AGB (t/ha)	Number	AGB (t/ha)	Number	AGB (t/ha)
01	129.252	11	80.171	21	172.128	31	54.836
02	142.776	12	174.936	22	166.592	32	167.011
03	139.653	13	147.477	23	98.417	33	165.710
04	58.508	14	153.008	24	104.223	34	144.930
05	166.223	15	185.083	25	151.198	35	109.724
06	4.248	16	177.771	26	164.641	36	95.931
07	113.727	17	163.469	27	180.735	37	24.281
08	79.486	18	157.807	28	102.843	38	33.292
09	29.471	19	65.888	29	150.238		
10	132.427	20	90.952	30	114.632		

3. Methods

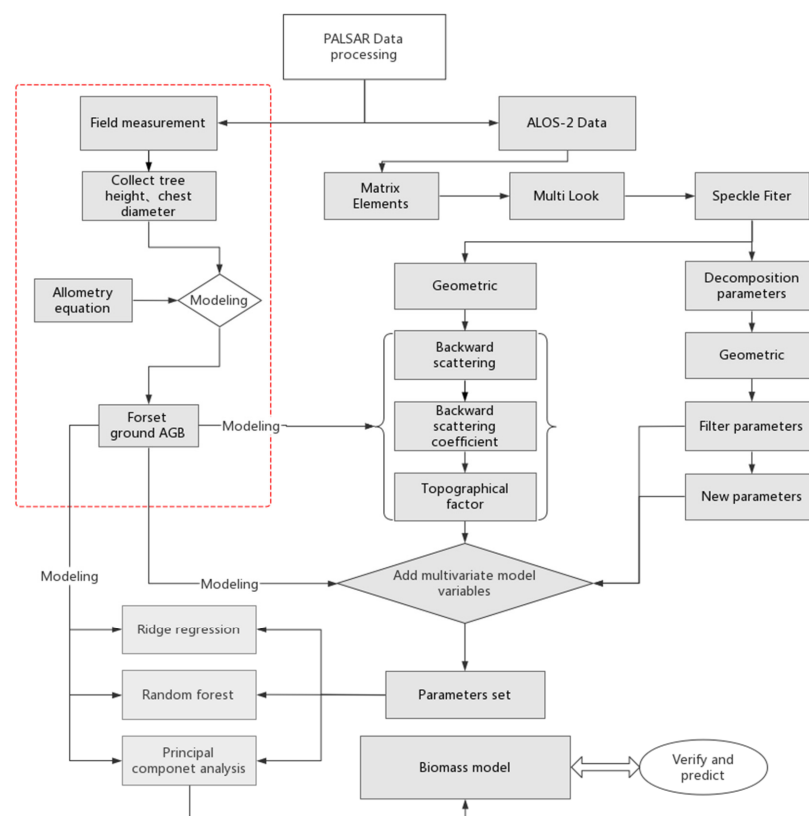The processing steps for field inventory and ALOS-2 PALSAR-2 data are shown in Figure 2.

Figure 2. Flowchart.

3.1. SAR Data Processing

Calibration: Conversion of the amplitude data record in the original image into a backscatter coefficient was not affected by changes in surface parameters. In order to expand the dynamic range of the scattering coefficient, the amplitude data record was expressed in decibels, as follows:

$$\sigma_{i,j}^0 = 10 \cdot \lg\left(DN_{i,j}^2\right) + CF_1. \tag{1}$$

where $\sigma_{i,j}^0$ is backscatter coefficients, $DN_{i,j}$ is the gray value of the pixel, and CF_1 is the calibration factor [42].

The four backscatter coefficients (σ_{HH}, σ_{HV}, σ_{VH}, and σ_{VV}) were obtained by radiation calibration.

Filter denoising: Given that SAR is a coherent system, speckle noise becomes an inherent feature that interferes with image readings. The present experiment used a refined Lee filter [43]. At the same time, multi-look processing also had a noise suppressing effect. Multi-look processing improved the effectiveness of feature information extraction by averaging the pixels of the SAR image azimuth and distance. A 4×9 multi-look process was performed on the original image to ensure that the pixels closed to the square and matched the area in the plot. The above process was run in the Gamma software [44].

Decomposition parameter acquisition: Since the research object was a distributed target, it was found suitable for incoherent decomposition. Three polarization decomposition methods suitable for forests were selected [45,46]. These methods included Yamaguchi three-component decomposition, eigenvalue-based H/A/alpha decomposition, and eigenvector-based H/A/alpha decomposition [47–53]. The Yamaguchi three-component decomposition method decomposes the echo signal into three scattering mechanisms, and volume scattering in the layered random medium provides good results [51]. H/A/alpha decomposition contains information about the dominance relationship between scattering mechanisms. Among them, the scattering entropy (H) not only represents the specific gravity of different scattering mechanisms in the whole scattering process, but also describes the randomness of the scattering process. The degree of heterogeneity in different directions (A) characterizes the degree of influence of the other two scattering mechanisms, which do not dominate the result when H increases. Scattering angle (α) describes the degree of freedom inside the target [54–56]. The polarization decomposition parameters were obtained using PolSARpro 6.0.2 [57].

Geocoding: Since SAR is a side-view system, it causes nonlinear distortion in areas with large terrain undulations. Therefore, SAR images cannot transform into a reference coordinate system by polynomial correction or affine transformation. The present study combined the imaging characteristics of the sensor and the ground morphology. It exploited external DEM data (SRTM V2 30 m resolution) and used a strict-range Doppler to geocode SAR image data. This process was run using Gamma software.

Thirty-five original polarization decomposition parameters were obtained through three polarization decompositions shown in Table 2 [49,50].

3.2. Backscatter Coefficient and Its Combination

The correlations between backscatter coefficients (σ_{HH}, σ_{HV}, σ_{VH}, σ_{VV}) and AGB were analyzed. The radar satisfied the reciprocity of a single station, thus the cross-polarization channels were averaged (σ_X replaces $\sigma_{(HV+VH)/2}$). Each variable was used to establish univariate linear models with AGB. The model was built using Matlab-2014b [58]. Meanwhile, different combinations of backscatter coefficients had different sensitivities to AGB [19]. We combined the backscatter coefficients to find the parameters with more significant correlations. A total of 26 different combinations were created using backscatter coefficients, and correlation analysis was performed for the 26 combinations. Significant variables were selected to establish univariate linear models with AGB.

Table 2. Decomposition parameters.

Method	Parameter	
Yamaguchi three-component decomposition	Odd scattering component of Yamaguchi 3 decomposition (Yamaguchi$_{Odd}$) Even scattering component of Yamaguchi 3 decomposition (Yamaguchi$_{Dbl}$) Scattering component of Yamaguchi 3 decomposition volume (Yamaguchi$_{Vol}$)	
H/A/alpha eigenvalue set decomposition	Eigenvalue	anisotropy, ansiotropy_lueneburg, anisotropy 12 asymetry, derd, derd_norm, entropysh, entropy 1 entropy 2, entropy 3, entropy 4, entropy 5, I1, I2, I3, p1, p2, p3, prdestal, polarisation_fraction rvi, serd, serd_norm
H/A/alpha eigenvector set decomposition	Eigenvector	alpha, alpha1, alpha 2, alpha 3 beta, beta 1, beta 2, beta 3 delta, delta 1, delta 2, delta 3 gamma, gamma1, gamma 2, gamma 3

3.3. Terrain Factors

Topography is an important factor that affects AGB [59–61]. This study obtained slope, aspect, and elevation using DEM, which were combined in Arcmap 10.7 as shown in Figure 3 [62]. The correlation between the extracted terrain factors and AGB was also analyzed.

(a)

(b)

(c)
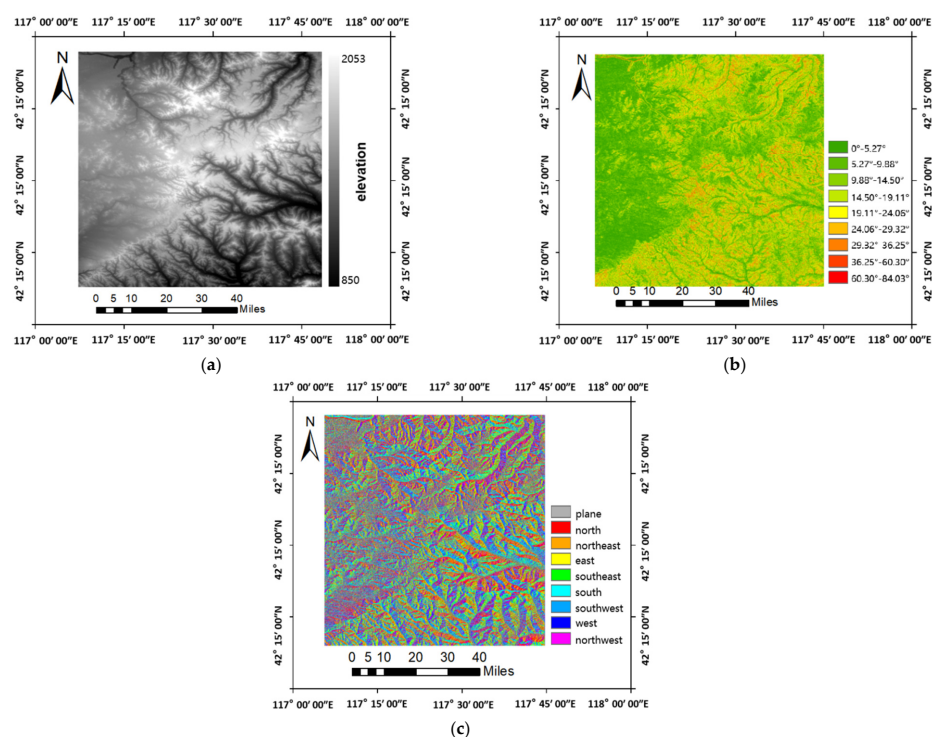
Figure 3. (**a**) Elevation; (**b**) slope; (**c**) aspect.

3.4. Constructing New Parameters

Previous studies have shown that the proportional combination of volume scattering, secondary scattering, and surface scattering has a certain sensitivity to forest canopy structure [63]. They derived a relationship between the growing stock volume (GSV) and polarimetric decomposition powers. In addition, these studies have found that the volumetric scattering power and GSV in different samples were all positively correlated, while the surface scattering and GSV were all negatively correlated. Therefore, it was concluded that the GSV and ratio of the three scattering powers have a certain sensitivity [64]. In the present study, there was a close relationship between AGB and GSV. The products of the different scattering mechanisms of the Yamaguchi three-component decomposition and the other two scattering mechanisms were found to possess a ratio relationship. This study established new parameters with reference to the above-mentioned study. Each new parameter with AGB was used to build a linear model. The construction of the new parameters was as follows:

- Ground scattering—scattering parameter ratio;

$$R_1 = \frac{Yamaguchi_{Odd}}{Yamaguchi_{Dbl} \times Yamaguchi_{Vol}}$$

- Even-scattering molecular parameters;

$$R_2 = \frac{Yamaguchi_{Dbl}}{Yamaguchi_{Odd} \times Yamaguchi_{Vol}}$$

- Volume-scattering molecular parameters.

$$R_3 = \frac{Yamaguchi_{Vol}}{Yamaguchi_{Dbl} \times Yamaguchi_{Odd}}$$

3.5. Multivariate Linear Model

The parameters obtained through the three polarization decomposition methods were not all applicable to the study of the forest. Therefore, we analyzed the correlation between decomposition variables and AGB to obtain significant correlation variables. A multivariate linear model with all the significant correlation variables was set up to predict AGB. The model variance inflation factor (VIF) test showed that the variables had significant multicollinearity.

3.6. Ridge Regression

Due to the complexity of the radar signal, there was a degree of information overlap between the variables, resulting in collinearity. This study attempted to use the ridge regression model to solve the collinearity problem. Ridge regression is a regularization method for the regression analysis of ill-posed problems.

3.7. Random Forest

The RF method is a classifier that consists of multiple decision trees. It belongs to the Bagging ensemble learning algorithm. This method was used to collect multiple sub-datasets from the original dataset and train multiple different decision trees. The prediction results of multiple decision trees were then averaged to obtain the final result. This method was not affected by collinearity between variables.

3.8. Principal Component Analysis

Principal component analysis (PCA) is suitable for populations of high-dimensional variables with a certain correlation between samples. There was collinearity in the above parameter set. Nevertheless, PCA is more suitable for removing collinearity [65]. The

principal components express the additive combination with the variance of each sample. The linear combination is added when the current component is not enough to represent the information of the original parameter set. The principal component was calculated as follows:

$$F_P = a_{1i} \times Z_{x1} + a_{2i} \times Z_{x2} + \cdots + a_{pi} \times Z_{xp} \tag{2}$$

$$A = (a_{ij})p \times m = (a_1, a_2, \cdots a_m), R_{ai} = \gamma_i a_i. \tag{3}$$

The eigenvector corresponding to the covariance matrix is $a_{1i}, a_{2i} \cdots a_{pi} (i = 1, \cdots m)$. $Z_{x1}, ZX_2 Z_{x2}, \cdots, Z_{xp}$ are the standard variables, R is the correlation coefficient matrix, and γ_i, a_i are the corresponding eigenvalue and eigenvectors.

We used IBM-SPSS 23.0 to perform principal component analysis on the dataset [66]. The two principal components were used to build a multivariate model to estimate AGB.

3.9. Verification and Prediction

Due to the small number of samples in this study, the cross-leave-one-out method was used for verification [67]. In total, 37 samples were used to model, and one sample was used for verification, resulting in 38 models. Through this method, the predicted AGB of SAR variables was obtained. Some of the evaluation indicators were used to describe the difference between the true AGB and the predicted AGB. The indicators selected in this study were goodness of fit (R^2), root mean square error (RMSE), mean absolute error (MAE), mean absolute percentage error (MARE), mean error (ME), and mean relative error (MRE) [68]. The best model was selected based on these indicators. The predicted biomass map was then obtained. The accuracy of the final model was referred to as the accuracy of the biomass map.

4. Results

4.1. Backscatter Coefficient and Its Combination

The correlation analysis between the backscatter coefficient and AGB (Table 3) showed that the horizontal cross-polarization in this region was more sensitive to AGB [9,11]. A univariate linear model was established between the backscatter coefficient and AGB (Figure 4). The accuracy of the model was low, and there were large deviations in estimating low-level AGB. The backscatter coefficient estimation of AGB was found to produce a saturation point, which led to greater limitations in the estimation results. The most accurate linear models were the σ_X and AGB. The formula of this model was AGB $= 280.394 + 12.591 \times \sigma_X$.

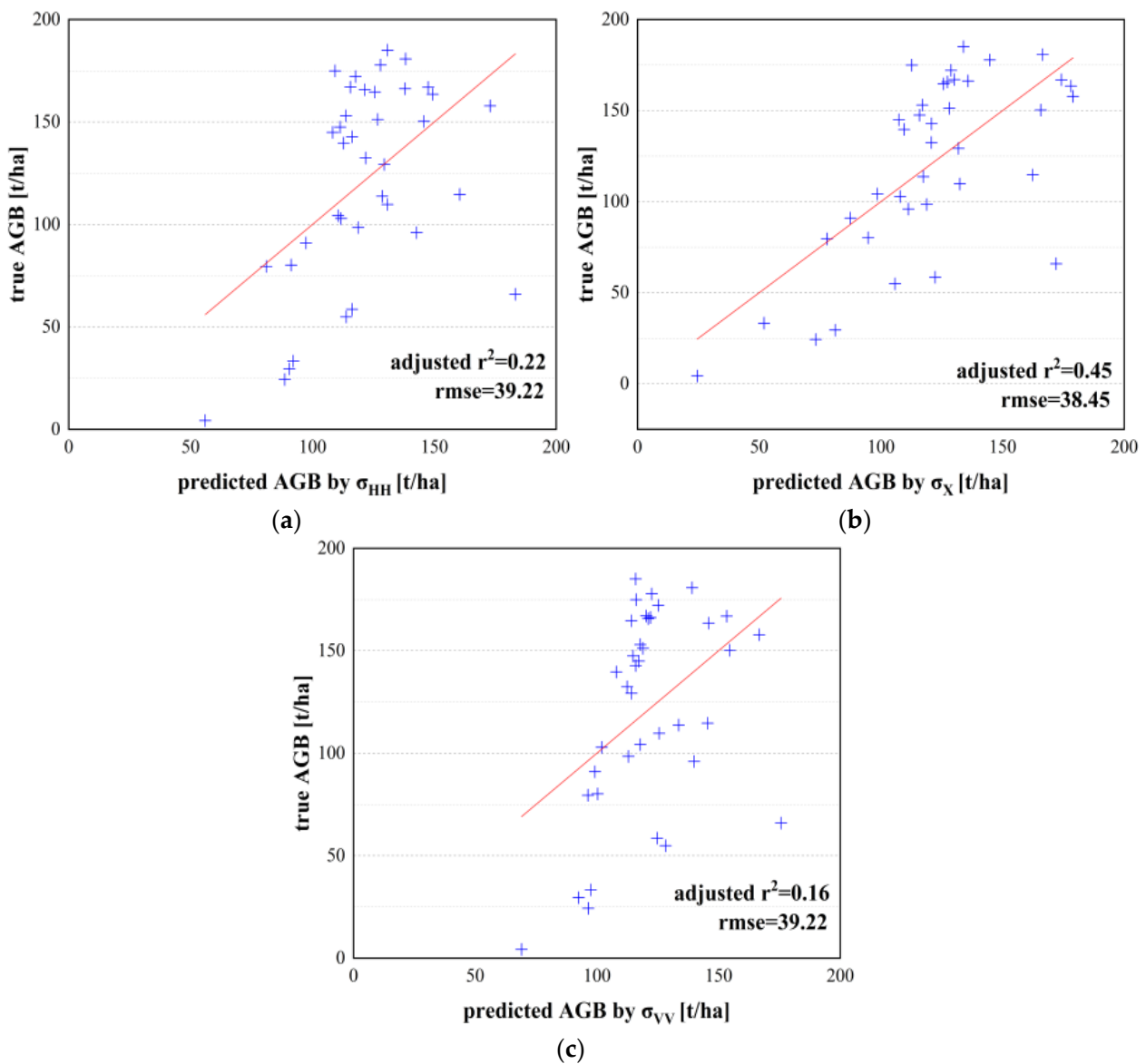**Table 3.** AGB backscatter coefficients correlation analysis.

Correlation Coefficient	Backscatter Coefficients		
	σ_{HH}	σ_X	σ_{VV}
Person coefficient	0.497 **	0.680 **	0.425 **

** Statistical significance: Statistical significance represents a significant correlation between the variables.

The backscatter coefficients were combined to determine whether they had the potential to improve AGB estimation (Table 4).

In this study, the combination of poorly correlated backscatter coefficients was not significant. The correlation of the three significantly correlated and newly combined variables ($\sigma_{HH \times VV}$, $\sigma_{HH \times X}$ and $\sigma_{HH \times X \times VV}$) was better than the σ_{HH} and σ_{VV} polarization channels. A univariate model with AGB was established for the three new variables (Figure 5). The most accurate were the $\sigma_{HH \times X \times VV}$ and AGB linear models. The formula of this model was AGB $= 152.822 + 0.039 \times \sigma_{HH \times X \times VV}$. However, it was found that the accuracy of these models was the same as that of the backscatter coefficient model. The saturation point of this model was about 125 t/ha.

(**a**)

(**b**)

(**c**)

Figure 4. (**a**) Models established by σ_{HH} and AGB; (**b**) models established by σ_X and AGB; (**c**) models established by σ_{VV} and AGB.

Table 4. AGB backscatter coefficients correlation analysis.

Parameter	Pearson Coefficient	Parameter	Pearson Coefficient	Parameter	Pearson Coefficient
$\sigma_{HH/VV}$	−0.154	$\sigma_{(VV+X)/HH}$	−0.060	σ_{VV+X}	0.102
$\sigma_{HH/X}$	−0.200	$\sigma_{(VV+X)/X}$	−0.093	σ_{HH-VV}	−0.217
$\sigma_{VV/X}$	−0.093	$\sigma_{(VV+X)/VV}$	0.144	σ_{HH-X}	0.243
$\sigma_{(HH+VV)/HH}$	0.043	$\sigma_{(HH+VV+X)/HH}$	−0.060	σ_{X-VV}	−0.263
$\sigma_{(HH+VV)/VV}$	−0.154	$\sigma_{(HH+VV+X)/X}$	0.143	$\sigma_{HH-VV-X}$	−0.232
$\sigma_{(HH+VV)/X}$	−0.148	$\sigma_{(HH+VV+X)/VV}$	−0.148	$\sigma_{HH\times VV}$	−0.637 **
$\sigma_{(HH+X)X}$	−0.200	σ_{HH+VV}	0.285	$\sigma_{X\times HH}$	−0.631 **
$\sigma_{(HH+X)/HH}$	−0.066	σ_{HH+X}	0.117	$\sigma_{HH\times X\times VV}$	0.666 **
$\sigma_{(HH+X)/VV}$	0.143	$\sigma_{HH+VV+X}$	0.244		

** Statistical significance: Statistical significance represents a significant correlation between the variables.
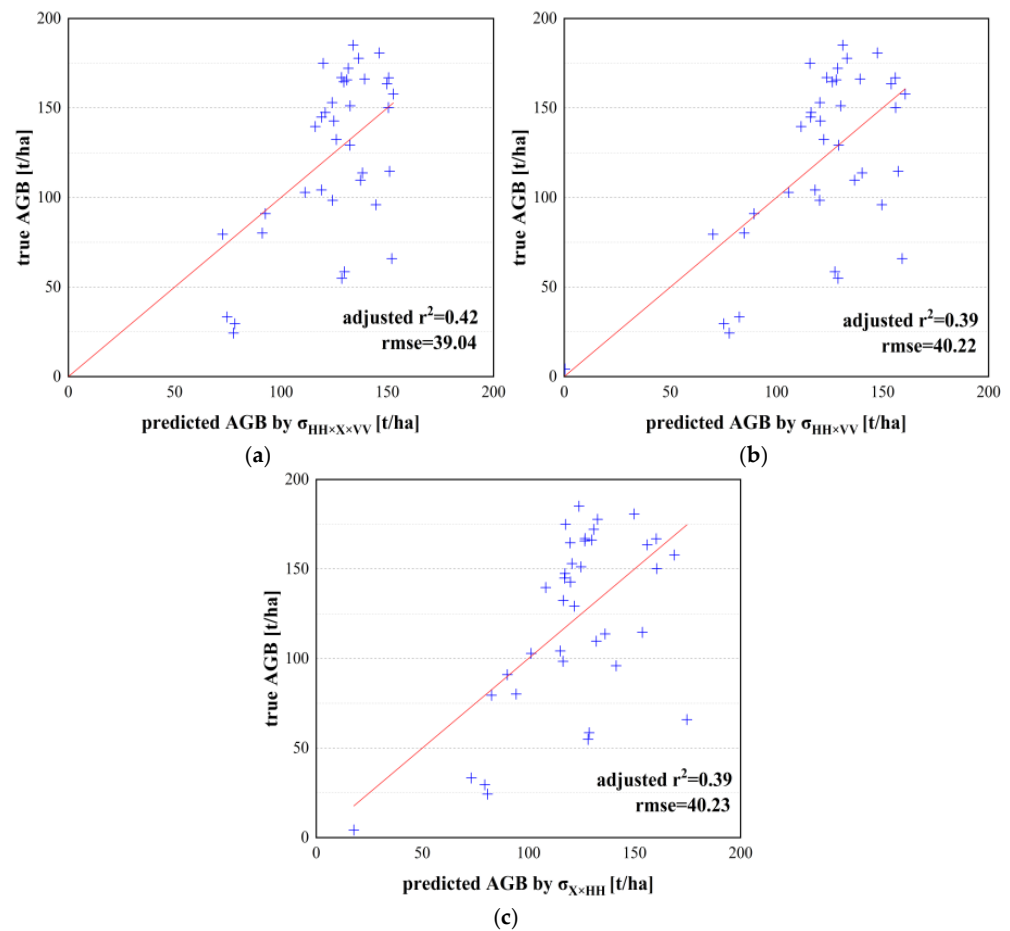
Figure 5. (**a**) Models established by $\sigma_{HH\times X\times VV}$ and AGB; (**b**) models established by $\sigma_{HH\times VV}$ and AGB; (**c**) models established by $\sigma_{X\times HH}$ and AGB.

4.2. Influence of Topographical Factors

Correlation analysis revealed that slope was the most important factor affecting AGB in this study (Table 5). During the field investigation, the slope of the study area was found to change greatly. However, the effect of aspect on AGB was not obvious, possibly due to the small number of samples.

Table 5. Topographical factors—AGB correlation analysis.

Parameters	Topographical Factors		
	Slope	Elevation	Aspect
Pearson coefficient	0.417 **	0.162	0.223

** Statistical significance: Statistical significance represents a significant correlation between the variables.

4.3. New Parameters and AGB Estimation

The correlation between the three newly constructed parameters and AGB was determined, and it is illustrated in Table 6. The univariate model with R_1 as the independent variable produced better AGB estimation results. The formula of this model was $AGB = 181.427 - 3.822 \times R_1$. This model achieved the highest accuracy among all univariate models. The new parameters R_2 and R_3 predicted that the AGB results were poor (Figure 6). The saturation point of the model was relatively high (140 t/ha) when compared to the backscattering coefficient model.

Table 6. Parameter correlation analysis.

Correlation Coefficient	New Parameter		
	R_1	R_2	R_3
Pearson coefficient	−0.756 **	−0.322	0.190

** Statistical significance: Statistical significance represents a significant correlation between the variables.
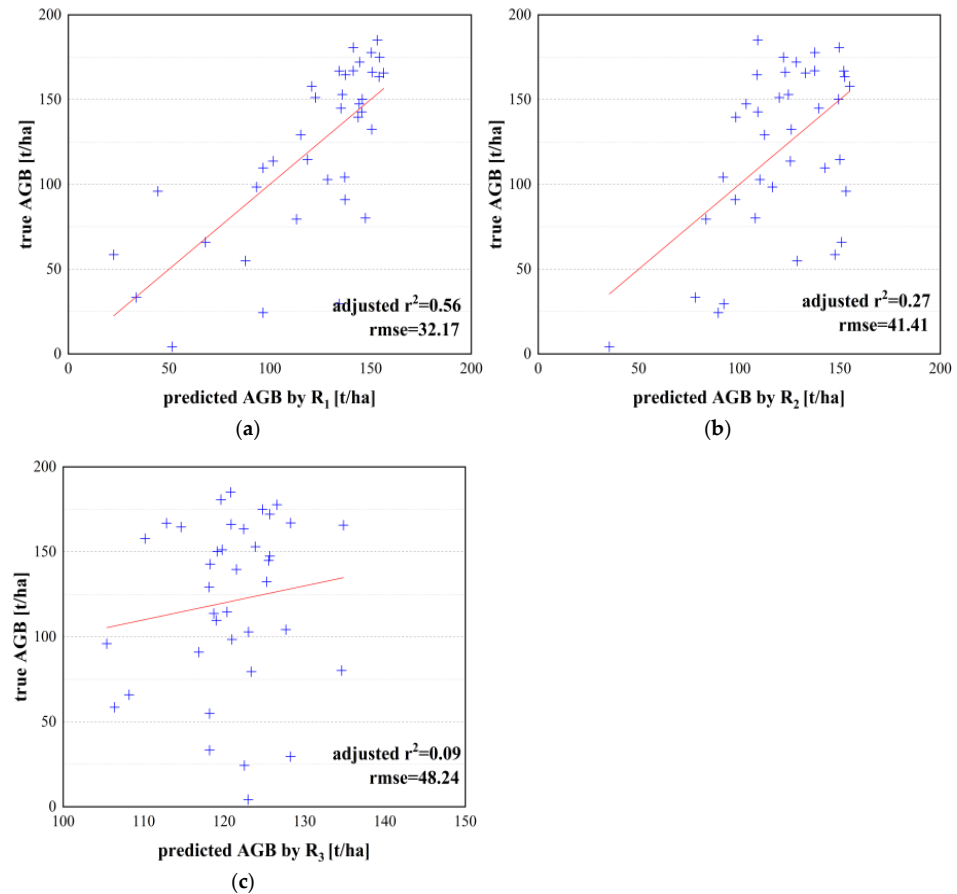
Figure 6. (**a**) Models established by R_1 and AGB; (**b**) models established by R_2 and AGB; (**c**) models established by R_3 and AGB.

### 4.4. Multivariate Linear Model

A correlation analysis of the polarization decomposition variables and AGB was performed, and it is summarized in Table 7 (only relevant significant variables are displayed). The variable R_1 had a stronger correlation with AGB compared to the Yamaguchi scattering mechanism. This showed that there was still a relationship between the mechanisms of polarization decomposition.

Table 7. AGB decomposition parameter correlation analysis.

Correlation Coefficient	Decomposition Parameter				
	Entropysh	Entropy 1	Entropy 2	Entropy 3	Gamma 3
Pearson coefficient	0.672 **	0.596 **	0.617 **	0.696 **	0.439 **
	I2	I3	Yamaguchi$_{Vol}$	Yamaguchi$_{Dbl}$	
Pearson coefficient	0.667 **	0.635 **	0.623 **	0.697 **	

** Statistical significance: Statistical significance represents a significant correlation between the variables.

All the variables that were significantly correlated with AGB were used to build a multivariate linear model (Figure 7). These variables included three original backscatter coefficients, three combined backscatter coefficients, slope, nine polarization decomposition variables, and R_1. However, the VIF test proved that there was multicollinearity between them (Table 8). The joint hypothesis F value of the model was 17.536, and there was no significant saturation point (sig) $\leq$ 0.001. This model provided poor residual test results (Figure 7). Meanwhile, existing studies have showed that AGB cannot be estimated with a simple multivariate model [69,70]. Although this model provided reasonable results, it could not predict AGB in large areas. The formula of this model was AGB $= -412.481 - 1.992 \times \sigma_{HH \times VV} - 612.789 \times$ Yamaguchi$_{vol} + 279.684 \times$ Yamaguchi$_{Dbl} - 819.198 \times$ Entropy $2 + 1359.506 \times$ I3 $+ 1693.609 \times$ I2 $+ 1051.944 \times$ Entropy 3 $+ 123.159 \times$ Entropy 1 $- 196.097 \times$ Entropysh $- 1.167 \times R_1 + 0.062 \times$ Gamma 3 $- 3.714 \times \sigma_{HH \times X} - 49.921 \times \sigma_{HH} - 5.658 \times \sigma_X - 412.481 \times \sigma_{VV} - 0.154 \times \sigma_{HH \times X \times VV}$.
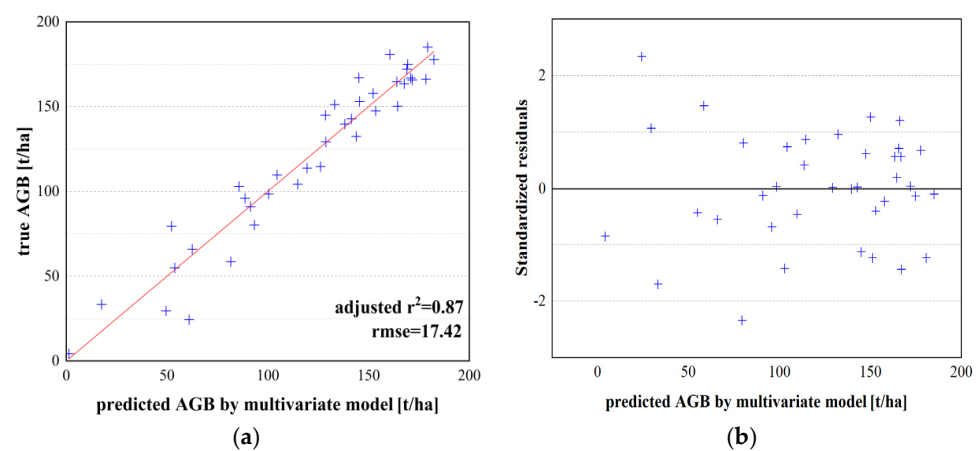
Figure 7. (**a**) Models established by all the variables that were significantly correlated; (**b**) residual analysis graph.

Table 8. Collinearity analysis.

Variable	Dimension	Sig	Vif
σ_{HH}	1	0.607	84.422
σ_X	2	0.251	689.347
σ_{VV}	3	0.925	150.481
$\sigma_{HH \times VV}$	4	0.150	346.537
$\sigma_{HH \times X}$	5	0.448	2571.564
$\sigma_{HH \times X \times VV}$	6	0.126	444.793
entropysh	7	0.656	1798.225
entropy 1	8	0.648	218.010
entropy 2_2	9	0.070	335.184
entropy 3_3	10	0.015	153.786
gamma 3	11	0.648	1.585
I2	12	0.535	295.838
I3	13	0.935	792.565
R_1	14	0.999	17.052
Yamaguchi$_{Vol}$	15	0.898	1125.782
Yamaguchi$_{Dbl}$	16	0.531	59.219

4.5. Ridge Regression Model

Ridge regression was used to estimate AGB and solve the collinearity problem. Variables in the ridge regression model were consistent with the multivariate model. The variables were standardized before ridge regression. However, the ridge regression model was found to have a poor fitting effect (Figure 8). This method solved the

collinearity between the variables. However, the normality of the residuals of the model was poor. Based on these results, the model estimated that the AGB saturation point was low (~145 t/ha). We determined the ridge parameter (K) = 0.141 based on the variance expansion factor method. The formula of this model was AGB = $83.396 - 0.161 \times \sigma_{HH \times VV} - 12.726 \times \text{Yamaguchi}_{vol} + 405.828 \times \text{Yamaguchi}_{Dbl} + 2.125 \times \text{Entropy } 2 - 13.587 \times \text{I3} + 78.432 \times \text{I2} + 50.428 \times \text{Entropy } 3 - 1.316 \times \text{Entropy } 1 + 0.805 \times \text{Entropysh} - 1.737 \times \text{R}_1 + 0.077 \times \text{Gamma } 3 - 0.065 \times \sigma_{HH \times X} - 1.446 \times \sigma_{HH} + 1.366 \times \sigma_X - 2.56 \times \sigma_{VV} + 0.009 \times \sigma_{HH \times X \times VV}$.
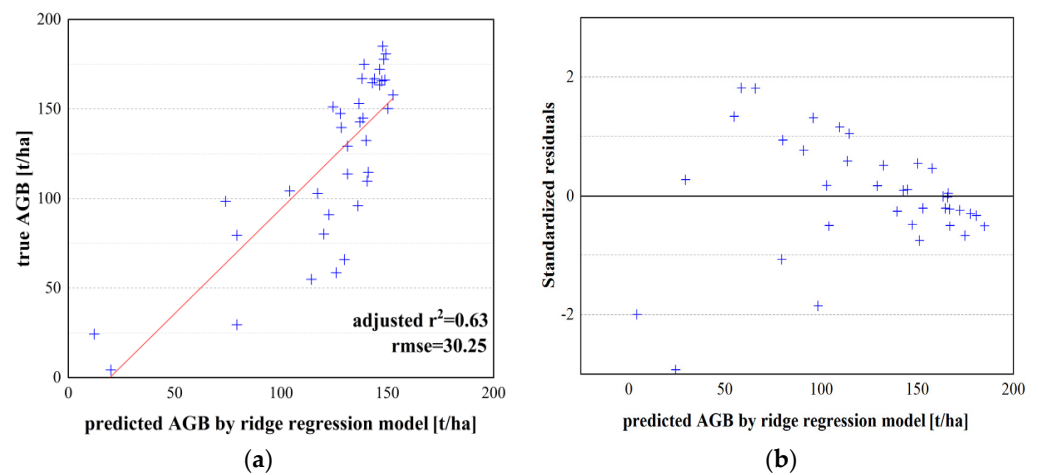

Figure 8. (**a**) Ridge regression model; (**b**) residual analysis graph.

4.6. Random Forest

There were 200 decision trees in this dataset. In order to reduce the result volatility caused by bootstrap sampling, all the models were trained 50 times and the average was obtained. We obtained the predicted AGB and computed the residuals (Figure 9). The saturation point of this model was about 155 t/ha.
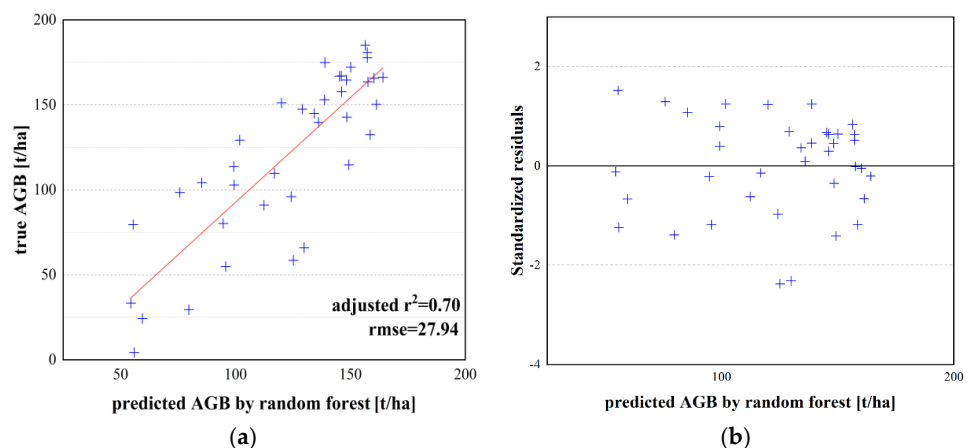

Figure 9. (**a**) Random forest model; (**b**) residual analysis graph.

4.7. Principal Component Analysis

Although the above results showed that multiple variables had the ability to improve AGB estimation, obtaining a stable model was still a challenge. However, the problem of collinearity can be solved through PCA. This method uses the same variable set as ridge regression. PCA processing was performed on the new parameter set. In addition, the Kaiser–Meyer–Olkin and Bartlett's tests were performed (Table 9), and the suitability of Kaiser–Meyer–Olkin sampling was between 0 and 1. A larger value indicated that it was

convenient for PCA. Bartlett's spherical significance test showed that the selection of the parameter population was suitable for PCA. We calculated the principal components by the principal component coefficients (Table 10). Two principal component variables were extracted by default. The cumulative variance described 80.606% of the original parameters (Table 11). Additionally, the AGB was estimated using a multivariate model (Figure 10). The formula of this model was AGB = 120.895 + 36.028 × Factor1 − 31.266 × Factor2. The F value of the multiple regressions model was 164.421, sig ≤ 0.001 (Table 12), and it passed the significance test, indicating a significant improvement in accuracy when compared with other multivariate models. PCA solved the problem of collinearity and the residuals of the model were normal. The residuals were evenly distributed, and thus the variance was considered to be homogeneous (Figure 9). All the results obtained through this model were acceptable.

Table 9. Kaiser–Meyer–Olkin and Bartlett's test.

Kaiser–Meyer–Olkin Sampling Suitability		0.746
Bartlett's Test	Approximated chi-square	1753.496
	Degree of freedom	136
	Significance	0.000

Table 10. Principal component coefficient.

Variable	Principal Component Coefficient	
	Factor 1	Factor 2
σ_{HH}	0.904	−0.310
σ_{X}	0.962	−0.305
σ_{VV}	0.900	−0.331
$\sigma_{HH \times VV}$	−0.915	0.237
$\sigma_{HH \times X}$	−0.933	0.209
$\sigma_{HH \times X \times VV}$	0.877	−0.185
entropysh	0.982	0.053
entropy 1	0.972	−0.056
entropy 2_2	0.966	0.082
entropy 3_3	0.953	−0.002
gamma 3	0.227	0.458
I2	0.924	0.240
I3	0.905	0.239
R_1	−0.349	−0.795
Yamaguchi$_{Vol}$	0.900	0.229
Yamaguchi$_{Dbl}$	0.847	0.287

Table 11. Illustration of the total variance.

Component	Eigenvalue			Cumulative		
	Aggregate	Variance (%)	Total (%)	Aggregate	Variance (%)	Total (%)
Factor 1	12.161	71.538	71.538	12.161	71.538	71.538
Factor 2	1.541	9.068	80.606	1.541	9.068	80.606

Table 12. Regression coefficients of the model.

Parameter	Unstandardized Coefficient	Student's Test Value	Sig	Vif
Constant	112.635	39.083	0.000	
Factor 1	34.427	10.982	0.000	1.000
Factor 2	−29.648	−9.458	0.000	1.000

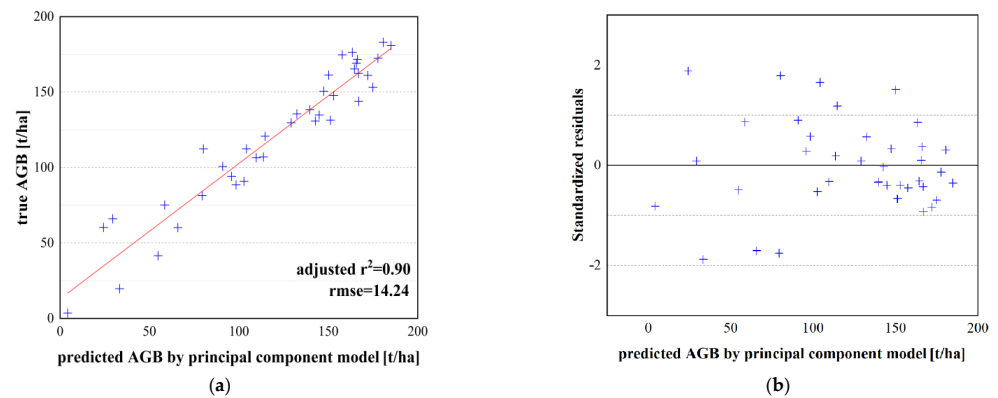**Figure 10.** (**a**) Models established by principal component analysis; (**b**) residual analysis graph.

4.8. Model Selection and Prediction of the Study Area AGB

We evaluated the relationship between the predicted AGB of each model and the real AGB (Table 13). This study concluded that the principal component model was the best model when compared with the evaluation indexes of the models. As such, the principal component model was used to predict the AGB in the study area (Figure 11). All the variable matrices required by the principal components were entered in Matlab2014b. All the matrices were additively combined according to the principal component coefficients to obtain the principal components. Finally, large-area AGB prediction was based on the multivariate model formula of the principal component. The accuracy of the biomass map was 88%.

Table 13. Model evaluation index.

| Type	Model	Evaluation Index					
		Adjusted r^2	RMSE (t/ha)	ME (t/ha)	MAE (t/ha)	MARE (%)	MRE (%)
Unary model	σ_X and AGB model	0.45	38.45	1.17	37.22	45.51	17.71
	$\sigma_{HH \times X \times VV}$ and AGB model	0.42	39.04	3.15	32.94	44.30	21.25
	R_1 and AGB model	0.56	32.17	1.82	25.69	39.17	8.77
	Multivariate model	0.87	17.42	−0.12	14.82	27.35	15.25
	Ridge regression model	0.63	30.25	−0.04	23.18	36.22	17.32
	Principal component model	0.90	14.24	−0.023	10.96	18.92	5.03
	Random forest model	0.70	27.94	−1.99	23.04	23.21	17.44
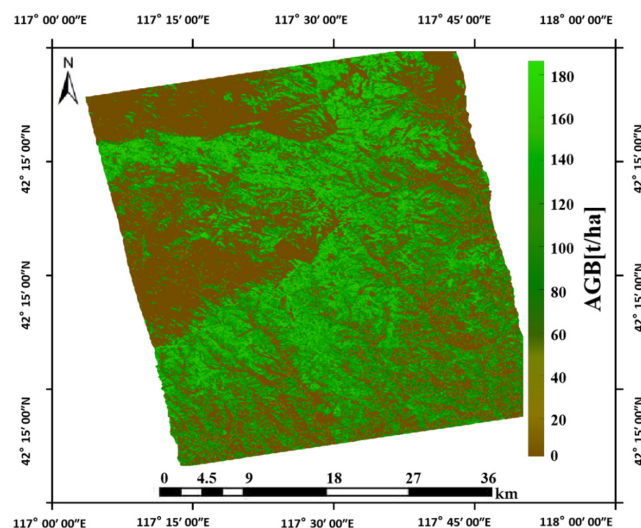
Figure 11. AGB prediction results.

5. Discussion

The use of large-scale remote sensing analyses to accurately estimate AGB is of great significance to global carbon-neutrality research. This study used a combination of backscatter coefficients, terrain parameters, and polarization decomposition parameters to estimate AGB. The adjusted r^2 increased from 0.45 to 0.90 through different processes. The accuracy of the processing results increased with the progress in various steps. The RMSE was 14.24 t/ha, as shown in step 4.6. Meanwhile, the ground information carried by the backscatter coefficient was limited. Therefore, AGB could not be accurately estimated. It was found that the combination of backscatter coefficients was more effective than HH and VV polarizations. Given that the topography of the study area was relatively complex, the slope was considered as an important factor affecting AGB. This study selected the polarization decomposition parameters that were suitable for forest AGB estimation. The univariate and the multivariate models were then compared. The results showed that the multivariate model estimates a high saturation point of the AGB. The saturation point of the backscattering coefficient was about 120 t/ha, and no obvious saturation point was estimated by the multivariate model. The saturation point of the variable R_1 was about 160 t/ha, which was higher than the backscattering coefficient model. This showed that the polarization decomposition parameters carried more ground information. The principal component analysis was found to be more suitable for the collinearity variable sets. As such, we used two principal components to build a multivariate model for estimating AGB without collinearity. No saturation point was found in this model, suggesting that the saturation point had been effectively improved. Finally, the principal component multivariate model was used to predict the AGB in our study area.

Previous reports have shown that the accuracy of the non-parametric model and the linear model is consistent in estimating AGB [71]. The accuracy of the multivariate model was proved to be higher than that of the univariate model [2]. Our findings were consistent with these previous findings. In the backscatter coefficient, cross-polarization had the strongest correlation with AGB [9,11]. The backscatter coefficient previously estimated the saturation point of AGB to be about 100 t/ha [17,18]. However, the saturation point of the backscattering coefficients in this study was higher than that previously reported. Many factors have been found to affect the saturation point of AGB [21]. For instance, variation in environmental conditions in a given study area was found to play a key role in causing variation in the saturation point [19]. Therefore, the different environments in our study area could have affected the saturation point. Reports have shown that the ratio of polarization backscattering coefficients has a high correlation with AGB [11]. However, the present study could not verify this finding. There is a possibility that no suitable combination of backscattering coefficients was found. Among several polarization decomposition methods, the most relevant parameter was Yamaguchi$_{Dbl}$. Yamaguchi$_{Dbl}$ represented the secondary scattering between forest trunks, and 90% of the forest AGB was tree trunks. These results are consistent with previously reported L-band characteristics [72]. Meanwhile, the Yamaguchi three-component decomposition corresponded to the physical model. In some aspects, the performance was better than the characteristic decomposition parameters. The several scattering mechanisms of the Yamaguchi three-component decomposition make it impossible to correctly distinguish land units. However, H/A/alpha decomposition provides a different decomposition method. The H/A/alpha polarization decomposition theorem is based on the coherence matrix analysis of eigenvalues and eigenvectors. The decomposed parameters describe the main relationship between the scattering mechanisms [45]. This suggests a lack of conflict between the two polarization decomposition methods. Previous studies showed a certain connection between the scattering mechanisms [64]. This finding is supported by the variable R_1 reported in the present study. In the present study, the RF method was found to be less effective and unsuitable for small sample studies. This was consistent with previous reports [39]. The additive model was found to be suitable for estimating AGB, as previously reported [27–29].

The L-band was used to obtain higher accuracy. This study showed that SAR data have the potential to estimate AGB, and are not limited by the saturation point of the estimated AGB. The unary model proved to be unsuitable for accurately estimating AGB. The multivariate model was proved to have a higher saturation point. However, the results estimated by principal component analysis were the closest to the real AGB. This study showed that AGB could be accurately estimated by one SAR image. However, the present research did not achieve such results; the obtained results were more suitable for the prediction of AGB in large areas.

Future studies could, however, use more penetrating P-band data, and select study areas with high biomass levels, such as tropical rain forests. Such studies may therefore enhance the ability to estimate AGB based on model selection. The present study employed an estimation technique that obtains better accuracy at the biomass level. It proved that estimating AGB using a combination of long-wave SAR data parameters and non-remote sensing factors can address actual needs. Although previous studies investigated polarization decomposition methods, the present study obtained better results due to the choice of images and reasonable processing methods used.

6. Conclusions

This study investigated the effectiveness of using an L-band image to estimate AGB. The obtained results could be widely applied to estimate AGB. The problem of complex radar signals that generate high-dimensional parameter sets was also addressed, further emphasizing the wide applicability of the method. The key findings of this study were as follows:

(1) The use of the backscatter coefficient to estimate AGB was more limited. The multivariate model provided better estimation capabilities than the univariate model. However, there was collinearity among the variables.

(2) The backscatter coefficient estimated that the AGB saturation point was low. The variable R_1 improved the estimation of the saturation point.

(3) The Earth-scattering ratio was more suitable for estimating AGB. This indicated that there was a degree of information complementarity between the variables. The combined backscatter coefficient was weak at estimating AGB.

(4) The model established by combining the backscatter coefficients, terrain factors, and polarization decomposition parameters achieved high accuracy. The principal component analysis method was suitable for analyzing SAR data to estimate AGB. The final model effectively improved the saturation point of AGB.

It is noteworthy that the study did not require a large amount of SAR data to accurately estimate AGB. L-band PALSAR data can be used in most areas of the world, making this research widely applicable to the estimation of AGB in forest-covered areas. However, the level of AGB in this study was not among the highest recorded in the world. Therefore, the applicability of this method in areas with high biomass levels is still uncertain.

Author Contributions: W.F. and Z.L. developed the research, conceived of, and designed the experiments. Z.L., Y.M., Y.H. and G.W. collected data for analysis. Z.L. and O.O.M. led the writing of the manuscript. W.F., O.O.M. and Z.L. contributed to the editing, revision, and discussion of the paper. All authors contributed critically to the drafts and gave final approval for publication. All authors have read and agreed to the published version of the manuscript.

Conflicts of Interest: The authors declare no conflict of interest. The founding sponsors had no role in the design of the study; in the collection, analyses, or interpretation of data; in the writing of the manuscript; or in the decision to publish the results.

References

1. Metcalf, C.J.E.; Graham, A.L.; Huijben, S.; Barclay, V.C.; Long, G.H.; Grenfell, B.T.; Read, A.F.; Bjørnstad, O.N. Partitioning Regulatory Mechanisms of Within-Host Malaria Dynamics Using the Effective Propagation Number. *Science* **2011**, *333*, 984–988. [CrossRef] [PubMed]
2. Tanase, M.A.; Panciera, R.; Lowell, K. Airborne multi-temporal L-band polarimetric SAR data for biomass estimation in semi-arid forests. *Remote Sens. Environ.* **2014**, *145*, 93–104. [CrossRef]
3. Blomberg, E.; Ferro-Famil, L.; Soja, M.J. Forest Biomass Retrieval From L-Band SAR Using Tomographic Ground Backscatter Removal. *IEEE Geosci. Remote Sens. Lett.* **2018**, *15*, 1030–1034. [CrossRef]
4. Sinha, S.; Jeganathan, C.; Sharma, L.K. Nathawat, M.S.; Das, A.K.; Mohan, S. Developing synergy regression models with space-borne ALOS PALSAR and Landsat TM sensors for retrieving tropical forest biomass. *J. Earth Syst. Sci.* **2016**, *125*, 725–735. [CrossRef]
5. Pulliainen, J.T.; Kurvonen, L.; Hallikainen, M.T. Multitemporal behavior of L- and C-band SAR observations of boreal forests. *IEEE Trans. Geosci. Remote Sens.* **1999**, *37*, 927–937. [CrossRef]
6. Baghdadi, N.; le Maire, G.; Bailly, J.-S.; Ose, K.; Nouvellon, Y.; Zribi, M.; Lemos, C.; Hakamada, R. Evaluation of ALOS/PALSAR L-Band Data for the Estimation of Eucalyptus Plantations Aboveground Biomass in Brazil. *IEEE J. Sel. Top. Appl. Earth Obs. Remote Sens.* **2015**, *8*, 3802–3811. [CrossRef]
7. Atwood, D.K.; Andersen, H.E.; Matthiss, B. Impact of Topographic Correction on Estimation of Aboveground Boreal Biomass Using Multi-temporal, L-Band Backscatter. *IEEE J. Sel. Top. Appl. Earth Obs. Remote Sens.* **2014**, *7*, 3262–3273. [CrossRef]
8. Caicoya, A.T.; Pardini, M.; Hajnsek, I.; Papathanassiou, K. Forest Above-Ground Biomass Estimation from Vertical Reflectivity Profiles at L-Band. *IEEE Geosci. Remote Sens. Lett.* **2015**, *12*, 2379–2383. [CrossRef]
9. Le Toan, T.; Beaudoin, A.; Riom, J.; Guyon, D. Relating forest biomass to SAR data. *IEEE Trans. Geosci. Remote Sens.* **1992**, *30*, 403–411. [CrossRef]
10. Rignot, E.; Way, J.; Williams, C.; Viereck, L. Radar estimates of aboveground biomass in boreal forests of interior Alaska. *IEEE Trans. Geosci. Remote Sens.* **1994**, *32*, 1117–1124. [CrossRef]
11. Ranson, K.; Sun, G. Mapping biomass of a northern forest using multifrequency SAR data. *IEEE Trans. Geosci. Remote Sens.* **1994**, *32*, 388–396. [CrossRef]
12. Eini-Zinab, S.; Maghsoudi, Y.; Sayedain, S.A. Assessing the performance of indicators resulting from three-component Freeman–Durden polarimetric SAR interferometry decomposition at P-and L-band in estimating tropical forest aboveground biomass. *Int. J. Remote Sens.* **2019**, *41*, 433–454. [CrossRef]
13. Golshani, P.; Maghsoudi, Y.; Sohrabi, H. Relating ALOS-2 PALSAR-2 Parameters to Biomass and Structure of Temperate Broadleaf Hyrcanian Forests. *J. Indian Soc. Remote Sens.* **2019**, *47*, 749–761. [CrossRef]
14. Asari, N.; Suratman, M.N.; Jaafar, J. Modelling and mapping of above ground biomass (AGB) of oil palm plantations in Malaysia using remotely-sensed data. *Int. J. Remote Sens.* **2017**, *38*, 4741–4764. [CrossRef]
15. Trisasongko, B.H.; Paull, D. A review of remote sensing applications in tropical forestry with a particular emphasis in the plantation sector. *Geocarto Int.* **2018**, *35*, 317–339. [CrossRef]
16. Ranson, K.J.; Sun, G.; Weishampel, J.F.; Knox, R.G. Forest biomass from combined ecosystem and radar backscatter modeling. *Remote Sens. Environ.* **1997**, *59*, 118–133. [CrossRef]
17. Kasischke, E.S.; Melack, J.M.; Dobson, M.C. The use of imaging radars for ecological applications—A review. *Remote Sens. Environ.* **1997**, *59*, 141–156. [CrossRef]
18. Yu, Y.; Saatchi, S. Sensitivity of L-Band SAR Backscatter to Aboveground Biomass of Global Forests. *Remote Sens.* **2016**, *8*, 522. [CrossRef]
19. Sarker, M.L.R.; Nichol, J.; Ahmad, B.; Busu, I.; Rahman, A.A. Potential of texture measurements of two-date dual polarization PALSAR data for the improvement of forest biomass estimation. *ISPRS J. Photogramm. Remote Sens.* **2012**, *69*, 146–166. [CrossRef]
20. Lal, P.; Kumar, A.; Saikia, P.; Das, A.; Patnaik, C.; Kumar, G.; Pandey, A.C.; Srivastava, P.; Dwivedi, C.S.; Khan, M.L. Effect of vegetation structure on above ground biomass in tropical deciduous forests of Central India. *Geocarto Int.* **2021**, *1*, 1–17. [CrossRef]
21. Baig, S.; Qazi, W.A.; Akhtar, A.M.; Waqar, M.M.; Ammar, A.; Gilani, H.; Mehmood, S.A. Above Ground Biomass Estimation of *Dalbergia sissoo* Forest Plantation from Dual-Polarized ALOS-2 PALSAR Data. *Can. J. Remote Sens.* **2017**, *43*, 297–308. [CrossRef]
22. Freeman, A.; Durden, S.L. A three-component scattering model for polarimetric SAR data. *IEEE Trans. Geosci. Remote Sens.* **1998**, *36*, 963–973. [CrossRef]
23. Zhang, Z.; Wang, Y.; Sun, G.; Ni, W.; Huang, W.; Zhang, L. Biomass Retrieval Based on Polarimetric Target Decomposition. In Proceedings of the IEEE International Geoscience and Remote Sensing Symposium, Vancouver, BC, Canada, 24–29 July 2011; pp. 1942–1945.
24. Bharadwaj, P.S.; Kumar, S.; Kushwaha, S.; Bijker, W. Polarimetric scattering model for estimation of above ground biomass of multilayer vegetation using ALOS-PALSAR quad-pol data. *Phys. Chem. Earth Parts A/B/C* **2015**, *83-84*, 187–195. [CrossRef]

25. Van Zyl, J.J.; Arii, M.; Kim, Y. Model-Based Decomposition of Polarimetric SAR Covariance Matrices Constrained for Nonnegative Eigenvalues. *IEEE Trans. Geosci. Remote Sens.* **2011**, *49*, 3452–3459. [CrossRef]

26. Verma, A.; Haldar, D. SAR polarimetric analysis for major land covers including pre-monsoon crops. *Geocarto Int.* **2019**, *36*, 2224–2240. [CrossRef]

27. Townsend, P.A. Estimating forest structure in wetlands using multitemporal SAR. *Remote Sens. Environ.* **2002**, *79*, 288–304. [CrossRef]

28. Santos, J.R.; Freitas, C.C.; Araujo, L.S.; Dutra, L.V.; Mura, J.C.; Gama, F.F.; Soler, L.S.; Sant'Anna, S.J. Airborne P-band SAR applied to the aboveground biomass studies in the Brazilian tropical rainforest. *Remote Sens. Environ.* **2003**, *87*, 482–493. [CrossRef]

29. Mougin, E.; Proisy, C.; Marty, G.; Fromard, F.; Puig, H.; Betoulle, J.; Rudant, J. Multifrequency and multipolarization radar backscattering from mangrove forests. *IEEE Trans. Geosci. Remote Sens.* **1999**, *37*, 94–102. [CrossRef]

30. Hyde, P.; Nelson, R.; Kimes, D.; Levine, E. Exploring LiDAR–RaDAR synergy—predicting aboveground biomass in a southwestern ponderosa pine forest using LiDAR, SAR and InSAR. *Remote Sens. Environ.* **2007**, *106*, 28–38. [CrossRef]

31. Wolpert, D.H.; Macready, W.G. An Efficient Method to Estimate Bagging's Generalization Error. *Mach. Learn.* **1999**, *35*, 41–55. [CrossRef]

32. Fu, W.; Guo, H.; Li, X. Relating Forest Biomass to the Polarization Phase Difference of the Double-Bounce Scattering Component. *IEEE Geosci. Remote Sens. Lett.* **2020**, *18*, 2048–2051. [CrossRef]

33. Sharifi, A.; Amini, J. Forest biomass estimation using synthetic aperture radar polarimetric features. *J. Appl. Remote Sens.* **2015**, *9*, 097695. [CrossRef]

34. Waqar, M.M.; Sukmawati, R.; Ji, Y.Q.; Sumantyo, J.T.S.; Segah, H.; Prasetyo, L.B. Retrieval of Tropical Peatland Forest Biomass from Polarimetric Features in Central Kalimantan, Indonesia. *Prog. Electromagn. Res. C* **2020**, *98*, 109–125. [CrossRef]

35. Huang, X.; Ziniti, B.; Torbick, N.; Ducey, M.J. Assessment of Forest above Ground Biomass Estimation Using Multi-Temporal C-band Sentinel-1 and Polarimetric L-band PALSAR-2 Data. *Remote Sens.* **2018**, *10*, 1424. [CrossRef]

36. Tanase, M.A.; Panciera, R.; Lowell, K.; Hacker, J.; Walker, J.P. Estimation of forest biomass from L-band polarimetric decomposition components. In Proceedings of the 2013 IEEE International Geoscience and Remote Sensing Symposium—IGARSS, Melbourne, VIC, Australia, 21–26 July 2013; pp. 949–952.

37. Gleason, C.J.; Im, J. Forest biomass estimation from airborne LiDAR data using machine learning approaches. *Remote Sens. Environ.* **2012**, *125*, 80–91. [CrossRef]

38. Mutanga, O.; Adam, E.; Cho, M.A. High density biomass estimation for wetland vegetation using WorldView-2 imagery and random forest regression algorithm. *Int. J. Appl. Earth Obs. Geoinf.* **2012**, *18*, 399–406. [CrossRef]

39. Fassnacht, F.; Hartig, F.; Latifi, H.; Berger, C.; Hernández, J.; Corvalán, P.; Koch, B. Importance of sample size, data type and prediction method for remote sensing-based estimations of aboveground forest biomass. *Remote Sens. Environ.* **2014**, *154*, 102–114. [CrossRef]

40. Sun, Z.; Liu, L.; Peng, S. Age-related modulation of the nitrogen resorption efficiency response to growth requirements and soil nitrogen availability in a temperate pine plantation. *Ecosystems* **2016**, *19*, 689–709. [CrossRef]

41. Wang, C. Biomass allometric equations for 10 co-occurring tree species in Chinese temperate forests. *For. Ecol. Manag.* **2006**, *222*, 9–16. [CrossRef]

42. Shimada, M.; Isoguchi, O.; Tadono, T. PALSAR radiometric and geometric calibration. *IEEE Trans. Geosci. Remote Sens.* **2009**, *47*, 3915–3932. [CrossRef]

43. Lee, J.-S.; Grunes, M.; De Grandi, G. Polarimetric SAR speckle filtering and its implication for classification. *IEEE Trans. Geosci. Remote Sens.* **1999**, *37*, 2363–2373. [CrossRef]

44. Gatelli, F.; Guamieri, A.M.; Parizzi, F. The wavenumber shift in SAR interferometry. *IEEE Trans. Geosci. Remote Sens.* **1994**, *32*, 855–865. [CrossRef]

45. Varghese, A.O.; Suryavanshi, A.; Joshi, A.K. Analysis of different polarimetric target decomposition methods in forest density classification using C band SAR data. *Int. J. Remote Sens.* **2016**, *37*, 694–709. [CrossRef]

46. Van Zyl, J.J. Application of Cloude's Target Decomposition Theorem to Polarimetric Imaging Radar Data. In Proceedings of the SPIE Volume 1748, Radar Polarimetry, San Diego, CA, USA, 22 July 1992; SPIE: Bellingham, WA, USA, 1993. [CrossRef]

47. Freeman, A. Fitting a Two-Component Scattering Model to Polarimetric SAR Data from Forests. *IEEE Trans. Geosci. Remote Sens.* **2007**, *45*, 2583–2592. [CrossRef]

48. Yamaguchi, Y.; Moriyama, T.; Ishido, M.; Yamada, H. Four-component scattering model for polarimetric SAR image decomposition. *IEEE Trans. Geosci. Remote Sens.* **2005**, *43*, 1699–1706. [CrossRef]

49. Yamaguchi, Y.; Yajima, Y.; Yamada, H. A Four-Component Decomposition of POLSAR Images Based on the Coherency Matrix. *IEEE Geosci. Remote Sens. Lett.* **2006**, *3*, 292–296. [CrossRef]

50. Yamaguchi, Y.; Sato, A.; Boerner, W.-M.; Sato, R.; Yamada, H. Four-Component Scattering Power Decomposition with Rotation of Coherency Matrix. *IEEE Trans. Geosci. Remote Sens.* **2011**, *49*, 2251–2258. [CrossRef]

51. Cui, Y.; Yamaguchi, Y.; Yang, J.; Park, S.-E.; Kobayashi, H.; Singh, G. Three-Component Power Decomposition for Polarimetric SAR Data Based on Adaptive Volume Scatter Modeling. *Remote Sens.* **2012**, *4*, 1559–1572. [CrossRef]

52. Cloude, S.R.; Pottier, E. Concept of polarization entropy in optical scattering. *Opt. Eng.* **1995**, *34*, 1599–1610. [CrossRef]

53. Touzi, R. Target Scattering Decomposition in Terms of Roll-Invariant Target Parameters. *IEEE Trans. Geosci. Remote Sens.* **2007**, *45*, 73–84. [CrossRef]

54. Hyde, P.; Dubayah, R.; Walker, W.; Blair, J.B.; Hofton, M.; Hunsaker, C. Mapping forest structure for wildlife habitat analysis using multi-sensor (LiDAR, SAR/InSAR, ETM+, Quickbird) synergy. *Remote Sens. Environ.* **2006**, *102*, 63–73. [CrossRef]

55. Zheng, D.; Rademacher, J.; Chen, J.; Crow, T.; Bresee, M.; Le Moine, J.; Ryu, S.-R. Estimating aboveground biomass using Landsat 7 ETM+ data across a managed landscape in northern Wisconsin, USA. *Remote Sens. Environ.* **2004**, *93*, 402–411. [CrossRef]

56. Cloude, R.S.; Pottier, E. An entropy based classification scheme for land applications of polarimetric SARs. *IEEE Trans. Geosci. Remote Sens.* **1997**, *35*, 68–78. [CrossRef]

57. Anconitano, G.; Lavalle, M.; Arabini, E. Sensitivity to soil moisture by applying a model-based polarimetric decomposition to a time-series of airborne radar L-band data over an agricultural area. *Microw. Remote Sens. Data Process. Appl.* **2021**, *11861*, 1186105. [CrossRef]

58. Simons-Legaard, E.; Legaard, K.; Weiskittel, A. Predicting aboveground biomass with LANDIS-II: A global and temporal analysis of parameter sensitivity. *Ecol. Model.* **2015**, *313*, 325–332. [CrossRef]

59. Mette, T.; Papathanassiou, K.; Hajnsek, I. Biomass estimation from polarimetric SAR interferometry over heterogeneous forest terrain. In Proceedings of the IEEE International Geoscience and Remote Sensing Symposium, Anchorage, AK, USA, 20–24 September 2004.

60. Sun, G.; Ranson, K.; Kharuk, V. Radiometric slope correction for forest biomass estimation from SAR data in the Western Sayani Mountains, Siberia. *Remote Sens. Environ.* **2002**, *79*, 279–287. [CrossRef]

61. Ojoyi, M.; Mutanga, O.; Odindi, J.; Abdel-Rahman, E.M. Application of topo-edaphic factors and remotely sensed vegetation indices to enhance biomass estimation in a heterogeneous landscape in the Eastern Arc Mountains of Tanzania. *Geocarto Int.* **2015**, *31*, 1–21. [CrossRef]

62. Aykut, T. Determination of groundwater potential zones using Geographical Information Systems (GIS) and Analytic Hierarchy Process (AHP) between Edirne-Kalkansogut (northwestern Turkey). *Groundw. Sustain. Dev.* **2021**, *12*, 100545. [CrossRef]

63. Lee, J.-S. Grunes, M.; Pottier, E.; Ferro-Famil, L. Unsupervised terrain classification preserving polarimetric scattering characteristics. *IEEE Trans. Geosci. Remote Sens.* **2004**, *42*, 722–731. [CrossRef]

64. Chowdhury, T.A.; Thiel, C.; Schmullius, C.; Stelmaszczuk-Górska, M. Polarimetric Parameters for Growing Stock Volume Estimation Using ALOS PALSAR L-Band Data over Siberian Forests. *Remote Sens.* **2013**, *5*, 5725–5756. [CrossRef]

65. Martínez, A.M.; Kak, A.C. PCA versus LDA. *IEEE Trans. Pattern Anal. Mach. Intell.* **2001**, *23*, 228–233. [CrossRef]

66. Castaño-Díaz, M.; Barrio-Anta, M.; Afif-Khouri, E.; Cámara-Obregón, A. Willow Short Rotation Coppice Trial in a Former Mining Area in Northern Spain: Effects of Clone, Fertilization and Planting Density on Yield after Five Years. *Forests* **2018**, *9*, 154. [CrossRef]

67. Wong, T.T. Performance evaluation of classification algorithms by k-fold and leave-one-out cross validation. *Pattern Recognit.* **2015**, *48*, 2839–2846. [CrossRef]

68. Quint, T.C.; Dech, J. Allometric models for predicting the aboveground biomass of Canada yew (*Taxus canadensis* Marsh.) from visual and digital cover estimates. *Can. J. For. Res.* **2010**, *40*, 2003–2014. [CrossRef]

69. Solberg, S.; Astrup, R.; Gobakken, T.; Næsset, E.; Weydahl, D.J. Estimating spruce and pine biomass with interferometric X-band SAR. *Remote Sens. Environ.* **2010**, *114*, 2353–2360. [CrossRef]

70. Wold, S.; Esbensen, K.; Geladi, P. Principal component analysis. *Chemom. Intell. Lab. Syst.* **1987**, *2*, 37–52. [CrossRef]

71. Neumann, M.; Saatchi, S.S.; Ulander, L.M.H.; Fransson, J.E.S. Assessing Performance of L- and P-Band Polarimetric Interferometric SAR Data in Estimating Boreal Forest Above-Ground Biomass. *IEEE Trans. Geosci. Remote Sens.* **2012**, *50*, 714–726. [CrossRef]

72. Kobayashi, S.; Omura, Y.; Sanga-Ngoie, K.; Widyorini, R.; Kawai, S.; Supriadi, B.; Yamaguchi, Y. Characteristics of Decomposition Powers of L-Band Multi-Polarimetric SAR in Assessing Tree Growth of Industrial Plantation Forests in the Tropics. *Remote Sens.* **2012**, *4*, 3058–3077. [CrossRef]